quires M⁺ 416.1776).

4-Benzoyl[2.2]paracyclophane (6). Benzoyl chloride (0.680 g, 4.84 mmol) and 0.58 g of aluminum chloride (4.34 mmol) were dissolved in 4.5 mL of 1,1,2,2-tetrachloroethane at room temperature. To the solution cooled to –30 °C, powdered [2.2]paracyclophane (0.500 g, 2.40 mmol) was added in one portion. The mixture was stirred at this temperature for 30 min and warmed to 0 °C over a period of 1 h. The solution was again cooled to –40 °C, 1.5 mL of 1N HCl was added, and the mixture was warmed slowly to 0 °C. Dichloromethane (50 mL) and water (20 mL) were added and the organic layer was separated and washed twice with water. After dichloromethane was evaporated 1,1,2,2-tetrachloroethane and unreacted benzoyl chloride were removed in vacuo (0.1 mm) on a water bath at 70 °C. The residue solidified and was recrystallized from ethanol to give colorless needles of 4-benzoyl[2.2]paracyclophane (717 mg, 96%): mp 126–128 °C; IR (KBr) 1650 cm⁻¹; MS, found M⁺ 312.1516 ($C_{23}H_{20}O$ requires M⁺ 312.1517); ¹H NMR (CDCl₃) δ 2.82–3.38 (m, 8 H), 6.34 (d, J = 8.1 Hz, 1 H), 6.53–6.58 (m, 3 H), 6.67–6.72 (m, 2 H), 6.75 (d, J = 7.6 Hz, 1 H), 7.40 (t, J = 8.1 Hz, 2 H), 7.53 (t, J = 8.1 Hz, 1 H), 7.71 (d, J = 8.1 Hz, 2 H).

Isomeric Cyclophane Dihydrazones (3a–c). Anhydrous hydrazine (2.0 mL) was added to the mixture of each dibenzoylcyclophane isomer (30 mg, 67.5 μmol), hydrazine monohydrochloride (50 mg, 1.37 mmol), and 3.0 mL of dry dimethyl sulfoxide. The mixture was heated at 110 °C for 8 h. After hydrazine and dimethyl sulfoxide were removed in vacuo at 80 °C, the residue was washed with water and dried in vacuo to give the corresponding dihydrazone in quantitative yield. For **3a**: mp 94–97 °C; MS, found M⁺ 444.2319 ($C_{30}H_{28}N_4$ requires M⁺ 444.2314). For **3b**: mp 93–105 °C; MS, found M⁺ 444.2319 ($C_{30}H_{28}N_4$ requires M⁺ 444.2314). For **3c**: mp 314–315 °C; MS, found M⁺ 444.2317 ($C_{30}H_{28}N_4$ requires M⁺ 444.2314).

4-Benzoyl[2.2]paracyclophane hydrazone was obtained quantitatively as a gummy solid from ketone 6 using the above method: MS, found M⁺ 326.1786 ($C_{23}H_{22}N_2$ requires M⁺ 326.1783).

***pseudo*-o-Bis(α-diazobenzyl)[2.2]paracyclophane (4a).** To a solution of pseudoortho dihydrazone **3a** (30 mg, 67.5 μmol) in 15 mL of benzene, 1.0 g (4.6 mmol) of mercuric oxide (yellow) and a few drops of a freshly prepared saturated solution of potassium hydroxide in absolute ethyl alcohol were added. After the mixture was stirred for 2 h at room temperature in the dark, the red solution was filtered through Celite and the residue washed with benzene. The combined benzene solutions were concentrated under reduced pressure in the cold. The residual solid was dissolved in 0.2 mL of benzene and placed on a disposable Pasteur pipet (146 mm, 5 mm i.d.) containing 1.6 g of alumina. The column was then rapidly washed with *n*-hexane–benzene (3:1) under moderate pressure.

The first eluted red solution was concentrated under reduced pressure in the cold to give 14 mg of pink powder of didiazo **4a** (47% yield). An analytical sample was recrystallized from *n*-hexane: mp 106–109 °C; IR (KBr) 2035 cm⁻¹; MS, found M⁺ – N₂ 412.1952 ($C_{30}H_{24}N_2$ requires M⁺ – N₂ 412.1939); UV–vis (2MTHF) λ_{max} 521 nm (log ε 2.44).

***pseudo*-m-Bis(α-diazobenzyl)[2.2]paracyclophane (4b).** Didiazo **4b** was prepared and purified as above. A red powder (12 mg, 40%) was obtained. An analytical sample was recrystallized from ether–petroleum ether (bp 30–70 °C): mp 136–138 °C (dec); IR (KBr) 2035 cm⁻¹; MS, found M⁺ – N₂ 412.1950 ($C_{30}H_{24}N_2$ requires M⁺ – N₂ 412.1939); UV–vis (2MTHF) λ_{max} 528 nm (log ε 2.39).

***pseudo*-p-Bis(α-diazobenzyl)[2.2]paracyclophane (4c).** Pseudopara dihydrazone **3c** (100 mg, 0.225 mmol) was dissolved in 50 mL of dichloromethane, and 4.0 g of mercuric oxide and a few drops of a freshly prepared saturated solution of potassium hydroxide in absolute alcohol were added to the solution. The mixture was stirred for 3 h at room temperature in the dark. After the solvent was removed by evaporation in the cold, the residual red solid was chromatographed on alumina deactivated water and eluted with dichloromethane to give 58 mg (59%) of scarlet crystals of didiazo **4c**. An analytical sample was recrystallized from CHCl₃–ether: mp 133–135 °C (dec); IR (KBr) 2035 cm⁻¹; MS, found M⁺ – N₂ 412.1914 ($C_{30}H_{24}N_2$ requires M⁺ – N₂ 412.1939); UV–vis (2MTHF) λ_{max} 521 nm (log ε 2.38).

4-(α-Diazobenzyl)[2.2]paracyclophane (7). To a solution of 4-benzoyl[2.2]paracyclophane hydrazone (200 mg, 0.613 mmol) in 40 mL of benzene, 5.0 g of mercuric oxide and a few drops of a freshly prepared saturated solution of potassium hydroxide in absolute alcohol were added. After the red solution was worked up, the residue was chromatographed as above to give 155 mg (78% yield) of red solid of diazo **7**. An analytical sample was recrystallized from petroleum ether (bp 30–70 °C): mp 103–105 °C; IR (KBr) 2040 cm⁻¹; MS, found M⁺ 324.1608 ($C_{23}H_{20}N_2$ requires M⁺ 324.1626); UV–vis (2MTHF) λ_{max} 525 nm (log ε 1.98); ¹H NMR (CDCl₃) δ 2.73–3.13 (m, 8 H), 6.33 (s, 1 H), 6.37–6.41 (m, 1 H), 6.52–6.64 (m, 5 H), 7.08 (t, J = 7.6 Hz, 1 H), 7.11 (d, J = 7.6 Hz, 2 H), 7.32 (t, J = 7.6 Hz, 2 H).

Carbon-13 Chemical Shielding Tensors in Polycyclic Aromatic Compounds. 1. Single-Crystal Study of Pyrene

Carl M. Carter, D. W. Alderman, Julio C. Facelli, and David M. Grant*

Contribution from the Department of Chemistry, University of Utah, Salt Lake City, Utah 84112. Received October 2, 1986

Abstract: The carbon-13 chemical shielding tensors measured in single-crystal pyrene are reported. The two internal bridgehead carbons have principal values of 197, 191, and –18 ppm and the four peripheral bridgehead carbons 213, 187, and –7 ppm with respect to liquid Me₄Si. The high field component of every tensor is determined to be perpendicular to the molecular plane, as in benzene. The protonated carbons have principal values similar to benzene, with the low-field components lying approximately along the C–H bonds. The rotation of the principal axes away from the C–H bond direction is measured experimentally and interpreted by quantum chemical calculations. By use of a MNDO wave function and the Pople model of chemical shielding, the magnitudes of the experimental in-plane components are reproduced very well and the calculated orientations of the principal axes are consistent with the experimental data. The results reported here demonstrate that the measurement of ¹³C shielding tensors in polycyclic aromatic compounds can be used as a measurement of the aromatic character of bonds adjacent to ¹³C nuclei.

With the advent of high-resolution ¹³C NMR in solids, the chemical shielding tensors of carbon nuclei have been studied in a few chemical environments.[1-3] Since the anisotropy in shifts

results from nonspherical distribution of electrons surrounding the nucleus, chemical shift tensors give new information about electronic structure and present a detailed three-dimensional view of important features of chemical bonding. The measured tensor

(1) Fyfe, C. A. *Solid State NMR for Chemists*; C.F.C.: Guelph, 1983.
(2) Mehring, M. *High Resolution NMR in Solids*, 2nd ed.; Springer: Berlin, 1983.

(3) Veeman, W. S. *Prog. NMR Spectrosc.* **1984**, *16*, 193.

2640   *J. Am. Chem. Soc., Vol. 109, No. 9, 1987*

Carter et al.
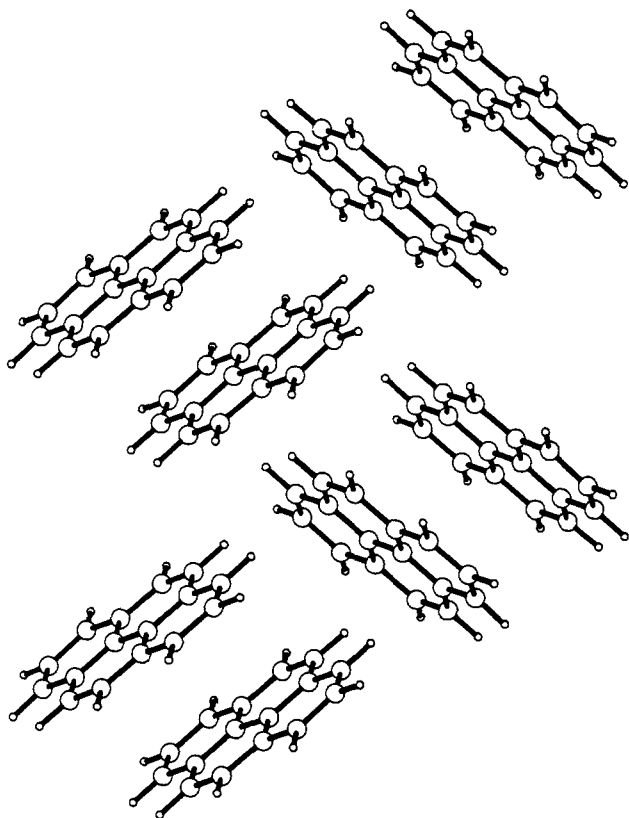
Figure 1. Pyrene unit cell projection on *ab* plane. The "crystallographic molecule" is a dimer pair of pyrene molecules.

reveals only the symmetric component of the shielding and can be diagonalized to obtain the three principal values and the directions of the three principal axes in the molecular frame.

Previous results[2-8] have shown that the measurement of ^{13}C shielding tensors can reveal an intimate relationship between shielding and molecular structure. In spite of the clear advantages of complete shielding tensors over the isotropic values, to our knowledge no shielding tensors have yet been reported for polycyclic aromatic hydrocarbons. Certainly this lack of information is not due to any lack of interest in this class of compounds. The importance of polycyclic aromatic compounds in many different chemical problems as well as the intrinsic theoretical interest in aromaticity is extremely well documented.[9-11] The lack of information on the ^{13}C shielding tensors in polycyclic aromatic compounds originates in the unusual experimental difficulties they present.

This paper reports the first measurement of ^{13}C shielding tensors of quaternary or bridgehead carbons in polycyclic aromatic compounds with a special emphasis given to the combined experimental and theoretical efforts needed to assign the data. The results provide a basis for understanding chemical shielding in

polycyclic aromatic compounds where the concept of aromaticity is of utmost importance.

The pyrene molecule was selected because of its two distinct bridgehead carbons, its high symmetry, and its ease of crystal growth. The crystal packing of pyrene molecules is shown in Figure 1. There are four pyrene molecules per unit cell arranged in two pairs of molecules which are identically oriented[12,13] and henceforth refered to as dimers. Proton second moment studies of solid pyrene show a C_2 rotation about the normal to the molecular plane with a correlation time of 10^{-5} s at 25 °C.[14,15] This motion is sufficiently rapid compared with the NMR time scale to average the otherwise nonequivalence of opposite ends of pyrene molecules implied by the crystal structure (see Figure 1). However, as this motion exchanges carbons related by inversion in the molecule, it averages only the intermolecular contribution to the chemical shift anisotropy (CSA).

In a single crystal each magnetically nonequivalent carbon in the unit cell produces a single relatively narrow line whose frequency is dependent upon the crystal orientation relative to the magnetic field. The anisotropy in the shielding is explored by rotating the crystal through a series of static positions. For a crystal rotated an angle θ_z about its z axis perpendicular to the magnetic field, it is easy to show[16] that the position of a line $\delta_{xy}(\theta_z)$ is given by

$$\delta_{xy}(\theta_z) = \frac{1}{2}(\sigma_{xx} + \sigma_{yy}) + \sigma_{xy} \sin 2\theta_z + \frac{1}{2}(\sigma_{xx} - \sigma_{yy}) \cos 2\theta_z \tag{1a}$$

For rotation about the x and y axes, the line positions are given by

$$\delta_{yz}(\theta_x) = \frac{1}{2}(\sigma_{yy} + \sigma_{zz}) + \sigma_{yz} \sin 2\theta_x + \frac{1}{2}(\sigma_{yy} - \sigma_{zz}) \cos 2\theta_x \tag{1b}$$

$$\delta_{zx}(\theta_y) = \frac{1}{2}(\sigma_{zz} + \sigma_{xx}) + \sigma_{zx} \sin 2\theta_y + \frac{1}{2}(\sigma_{zz} - \sigma_{xx}) \cos 2\theta_y \tag{1c}$$

From these three orthogonal rotations, the six symmetric elements of the tensor are fully determined. At this point the tensor components are in the bulk crystal or sample reference frame. Diagonalizing the matrix yields the principal values and the orientation of the principal axes system (PAS) in the sample frame. Usually X-ray data on the sample are needed to relate the crystallographic axes to the sample frame, and the crystal point symmetry and molecular symmetry are then used to transform the data into the molecular reference frame.

Experimental Section

A single crystal grown from sublimed pyrene (commercially obtained) by thermal convection in cyclohexane was gound to fill the volume enclosed by three intersecting orthogonal cylinders. This unique sample shape maximized the filling factor and accommodated the use of a 5-mm high-resolution NMR tube as a sample holder in the single-axis goniometer. The crystal was inserted along each of its three orthogonally ground axes and rotated perpendicular to the magnetic field. A 9° angular increment was used to obtain the three 180° rotational patterns.

All of the ^{13}C spectra were taken at 50.25 MHz on a Bruker CXP-200 spectrometer at room temperature. The probe was a modified double-tuned solids unit with the spinner assembly replaced with a single-axis goniometer constructed from a commercial high-precision brass worm gear set[17] held in a delrin assembly. High-resolution solid-state spectra are obtained by using the combined techniques of high-power proton decoupling and cross polarization;[18] FID signals were accumulated 20–40

(4) Strub, H.; Beeler, A. J.; Grant, D. M.; Michl, J.; Cutts, P. W.; Zilm, K. W. *J. Am. Chem. Soc.* **1983**, *105*, 3333.

(5) Facelli, J. C.; Orendt, A. M.; Beeler, A. J.; Solum, M. S.; Depke, G.; Malsch, K. D.; Downing, J. W.; Grant, D. M.; Michl, J. *J. Am. Chem. Soc.* **1985**, *107*, 6749. Facelli, J. C.; Orendt, A. M.; Solum, M. S.; Depke, G.; Grant, D. M.; Michl, J. *J. Am. Chem. Soc.* **1986**, *108*, 4268. Solum, M. S.; Facelli, J. C.; Michl, J.; Grant, D. M. *J. Am. Chem. Soc.* **1986**, *108*, 6464.

(6) Orendt, A. M.; Facelli, J. C.; Grant, D. M.; Michl, J.; Wlaker, F. H.; Dailey, W. P.; Waddel, S. T.; Wiberg, K. B.; Schindler, M.; Kutzelnigg, W. *Theor. Chim. Acta* **1985**, *68*, 421.

(7) Takegoshi, K.; McDowell, C. A. *Chem. Phys. Lett.* **1986**, *123*, 159; *J. Am. Chem. Soc.* **1986**, *108*, 6852.

(8) Takegoshi, K.; Naito, A.; McDowell, C. A. *J. Magn. Reson.* **1985**, *65*, 34.

(9) Bjorseth, A. *Handbook of Polycyclic Aromatic Hydrocarbons*; Marcel Dekker: New York, 1983.

(10) *Aromaticity, Pseudo-Aromaticity, Anti Aromaticity*; Bergman, E. D., Pullman, G., Eds.; Israel Academy of Sciences: Jerusalem, 1971.

(11) Herndom, W. C. *J. Am. Chem. Soc.* **1973**, *95*, 2404.

(12) Camerman, A.; Trotter, J. *Acta Crystallogr.* **1965**, *18*, 636.

(13) Hazell, A. C.; Larsen, F. K.; Lehmann, M. S. *Acta Crystallogr.* **1972**, *28*, 2977.

(14) Fyfe, C. A.; Gilson, D. F. R.; Thompson, K. H. *Chem. Phys. Lett.* **1970**, *5*, 215.

(15) Fyfe, C. A. *J. Chem. Soc., Faraday Trans. 2* **1974**, *70*, 1633.

(16) Spiess, H. W. *NMR Basic Principles and Progress*; Springer: Berlin, 1978; Vol. 15.

(17) Purchased from Winfred M. Berg. Inc., East Rockaway, NY.

(18) Pines, A.; Gibby, M. G.; Waugh, J. S. *J. Chem. Phys.* **1973**, *59*, 569.

13C Chemical Shielding Tensors

J. Am. Chem. Soc., Vol. 109, No. 9, 1987 2641
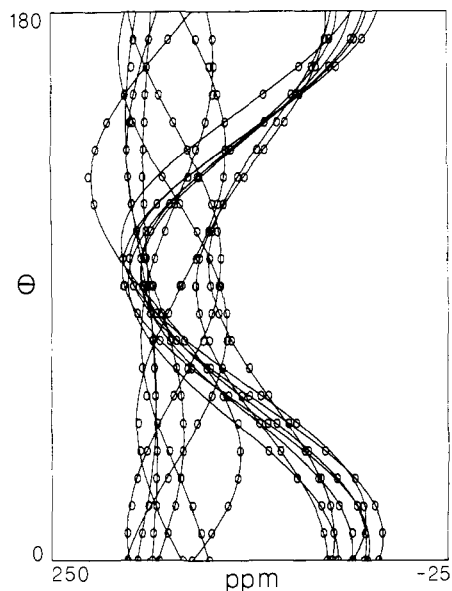
Figure 2. Representative rotation pattern of single-crystal pyrene. The division of the assignment problem in half is clearly illustrated. One molecule is sampled very nearly in the molecular plane by this rotation. The anisotropy between the in-plane components is relatively small, and the lines move relatively little. The other molecule is being rotated in and out of the molecular plane. This samples a greater range of the anisotropy, and the lines are seen to move much further.

times by using a Hartmann-Hahn match[19] with a 2-ms contact time, a repetition time of 826 s, and proton decoupling field of $\gamma H_2 = 175$ kHz in the rotating frame.

The ^{13}C chemical shifts are reported relative to Me$_4$Si by taking the ^{13}C shifts of solid adamantane (38.7, 29.5 ppm) as an external reference standard. By convention the lowest field principal value is designated as σ_{11} and the highest field is σ_{33}, so that in ppm downfield from Me$_4$Si, $\sigma_{11} > \sigma_{22} > \sigma_{33}$.

Though there are 64 carbon nuclei per unit cell, a maximum of 16 lines was observed experimentally as a consequence of both symmetry and motion. The symmetry of an isolated pyrene molecule is such that carbons related by inversion must have equivalent tensors. Thus, for a stationary pyrene molecule, up to eight carbon lines would be seen. Neighboring molecules in the crystal, however, are positioned so as to destroy the molecule's inversion symmetry, making all the carbons inequivalent, increasing the potential number of lines to 16 per molecule. At room temperature, however, every pyrene molecule in the crystal undergoes a rotation about a C_2 axis perpendicular to the molecular plane and through its inversion center which is sufficiently rapid to exchange the otherwise inequivalent ends of the molecule. This motion averages the intermolecular effects and reequates carbons related by the inversion center so that each $C_{16}H_{10}$ molecule will contribute only eight lines to the spectrum. Further, the equivalent positioning of both molecules in the so-called dimer renders the eight line spectra of these two molecules identical. Nonequivalence between the two dimers in the unit cell then doubles to 16 the number of observed resonance lines.

The positions of the 16 lines were traced for each of the three orthogonal patterns, and the sine, cosine, and constant coefficients of eq 1a-c were determined by a least-squares simplex fitting routine. A representative rotation pattern is shown in Figure 2. To follow each line in the three rotations, the intersections were tentatively identified by matching spectra and determined accurately by a second least-squares simplex routine. To correct minor discrepancies in the orthogonality of the three axes, the Euler angles defining the relationship of the rotation axes were parameterized in the second fitting routine. This analysis yielded all 16 shielding tensors. The matrices were then diagonalized to produce the principal values and their directions in the sample frame. The experimentally determined principal values are shown in Figure 3.

The eight carbons in a pyrene molecule producing distinct lines in the solid are labeled C_1, C_2, C_3, C_4, C_{10}, C_{3a}, C_{10a}, and C_{10b} in the Chart I. While carbons C_1 and C_3, carbons C_4 and C_{10}, and carbons C_{3a} and C_{10a} are chemically equivalent and thus have the same principal values, it is important to note that each pair of related carbons is magnetically nonequivalent and has different, but symmetry related, orientations of their principal axes.

(19) Hartmann, S. R.; Hahn, E. L. *Phys. Rev.* **1962**, *128*, 2042.
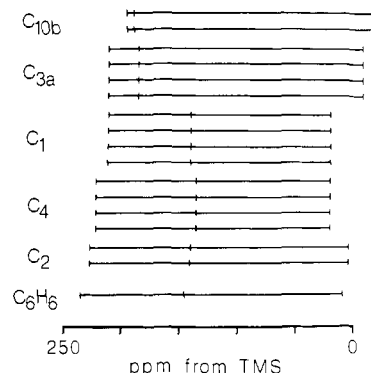
Figure 3. Experimentally determined pyrene principal values. Two groups of two and three groups of four are evident. The assignments are discussed in the text. Benzene (C_6H_6) principal values are included for comparison.

Chart I
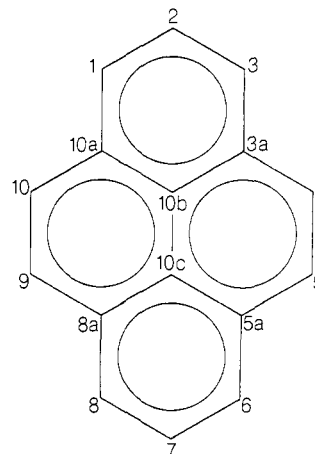
The high symmetry of the pyrene molecule greatly facilitates both the determination of the crystallographic axes and the assignment of the tensors directly from the NMR data. Because the liquid chemical shifts of pyrene are all within 7 ppm of one another,[20] the isotropic shifts are of limited help in making assignments. Rather the assignments were made from agreement in principal values, their orientations, and the number of their occurrences. Also, many of the tensors have principal values close to those of benzene, which has $\sigma_{11} = 234$ ppm along the C–H bond, $\sigma_{22} = 146$ ppm for the in-plane component perpendicular to the C–H bond, and $\sigma_{33} = 9$ ppm normal to the plane of the ring.[4] These similarities assist with the assignment of orientation of the principal axes for protonated carbons.

The experimentally determined directions of the principal axes associated with the σ_{33} components for all carbons in the pyrene crystal fall into two distinct groups of eight. The average angle between these two groups is 83.6° (±1.6°) with only a few degrees scatter within each group. The neutron diffraction study of pyrene[13] gives an angle of 83.3° between the normals to the molecular planes. Previous studies have shown the σ_{33} components of aromatic carbons to be consistently perpendicular to the aromatic ring.[2-4] Thus, the two directions of the σ_{33} components measured in the pyrene crystal are interpreted as the directions normal to the molecular planes. Tensors with the same σ_{33} direction are then associated with a given dimer, and the assignment problem is cleanly divided in half. As the σ_{33} directions define the normals of the two different molecular planes in the crystal frame, they provide the crystallographic orientation of the sample crystal.

Two nearly axially symmetric tensors with principal values $\sigma_{11} = 197$, $\sigma_{22} = 191$, and $\sigma_{33} = -18$ ppm are present, each having different σ_{33} orientations, so that they are from the two different dimers. A second pair of tensors with principal values $\sigma_{11} = 226$, $\sigma_{22} = 140$, and $\sigma_{33} = 4$ ppm are also present, one from each dimer. Since there is only one of each of these tensors per dimer, they can come only from the C_2 or C_{10b}. Because of its central position in the planar molecule, C_{10b} should be almost axially symmetric, while the C_2 environment is similar to the carbons in benzene. On this basis the $\sigma_{11} = 197$, $\sigma_{22} = 191$, and $\sigma_{33} =$

(20) Alger, T. D.; Grant, D. M.; Paul, E. G. *J. Am. Chem. Soc.* **1966**, *88*, 5397.
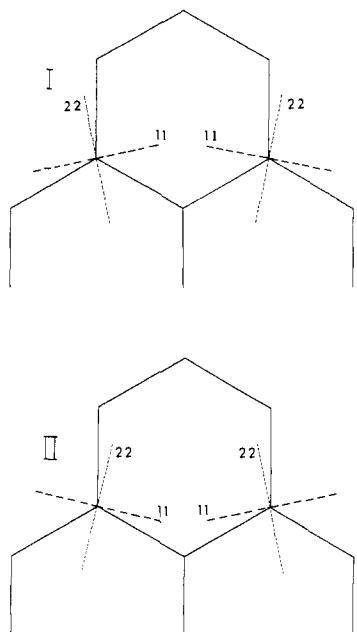
Figure 4. Alternative possibilities for the orientation of the in-plane principal axes of C_{3a} and C_{10a}. The calculations verify alternative I.

−18 ppm tensor is assigned to C_{10b} and the $\sigma_{11} = 226$, $\sigma_{22} = 140$, and $\sigma_{33} = 4$ ppm tensor to C_2. The molecular symmetry requires that one of the in-plane principal axes of both C_2 and C_{10b} lies along the long axis of the molecule parallel to the C_2–H bond. The $\sigma_{11} = 226$ ppm principal axis of C_2 is measured to lie along the C–H bond, as in benzene. It is the $\sigma_{11} = 197$ ppm principal axis of the C_{10b} tensor which is measured to be colinear with the C_2–H bond and thus also lies along the long axis of the molecule.

Four carbons with the second most axially symmetric tensors have principal values $\sigma_{11} = 213$, $\sigma_{22} = 187$, $\sigma_{33} = -7$ ppm, two from each dimer. They are assigned to the C_{3a} and C_{10a}, bridgehead carbons, which would be expected to be more axially symmetric than a protonated or benzene type tensor but less axially symmetric than for C_{10b}. The σ_{11} axes for the similar tensors from each dimer lie 78° in opposite directions from the long axis of the molecule. There is, unfortunately, no experimental evidence nor molecular symmetry to define which of the tensors comes from C_{3a} and which from C_{10a}. This assignment ambiguity results in the uncertainty in the orientation of the in-plane principal axes illustrated in Figure 4.

For the remaining carbons, the directions of the σ_{11} axes and the similarity of the principal values to those of benzene can be used to make further assignments. There are four tensors, two from each dimer, whose σ_{11} axes lie 58° in opposite directions from the long axis of the molecule, with principal values $\sigma_{11} = 212$, $\sigma_{22} = 141$, and $\sigma_{33} = 21$ ppm. These are tentatively assigned to C_1 and C_3 with the σ_{11} axes 2° from an idealized C–H bond direction. The last four tensors, two from each dimer, those σ_{11} axes lie 75° in opposite directions from the long axis of the molecule, have principal values of $\sigma_{11} = 222$, $\sigma_{22} = 136$, and $\sigma_{33} = 21$ ppm. These are tentatively assigned to C_4 and C_{10} with the σ_{11} axes 15° from the C–H bonds.

Calculations

In order to obtain information on the origin of chemical shielding in fused aromatic ring systems and to resolve the ambiguities in the assignment of carbons 3a and 10a and also carbons 3 and 4 of the measured ^{13}C shielding tensors of pyrene, simple quantum mechanical calculations were performed.

The limitations of current computational resources discourages the application of ab initio methods[5,21] in calculating shielding tensors of molecular systems as large as pyrene. It is well documented that semiempirical approaches can be used successfully to reproduce experimental trends within a series of related compounds.[22] Further, it is known that the diamagnetic contributions to the shielding tensor do not contribute significantly to the chemical shift or to the anisotropy of the shielding tensor.[22]

Consequently, it is necessary to consider only the paramagnetic contributions.

By use of the well-established Pople model for the isotropic chemical shielding,[23,24] the paramagnetic contribution to the shielding of the A nucleus is given by

$$[\sigma^{(p)}]_{\alpha\beta} = -K \sum_{j}^{occ} \sum_{k}^{unocc} (^1E_j - {}^1E_0)^{-1} \times$$

$$\sum_{\mu<\nu}^{A} \sum_{B} \sum_{\lambda<\sigma}^{B} (C_{\mu j}C_{\nu k} - C_{\nu j}C_{\mu k})(C_{\lambda j}C_{\sigma k} - C_{\sigma j}C_{\lambda k})\langle\phi_\mu|r^{-3}L_\alpha|\phi_\nu\rangle \times$$

$$\langle\phi_\lambda|L_\beta|\phi_\sigma\rangle \quad (2)$$

$$K = \frac{\mu_0 e^2 \hbar^2}{2\pi m^2}$$

where the usual notation is used.[22] If only s and p orbitals are used in the basis set, only local terms are included in the calculation, the ΔE approximation is taken, and the closure relationship for a ZDO[25] wave function

$$\sum_{j}^{occ} C_{\mu j}C_{\lambda j} + \sum_{k}^{unocc} C_{\mu k}C_{\lambda k} = \delta_{\mu\lambda} \quad (3)$$

is used, it becomes a relatively simple matter to extend the Pople model to individual tensor shielding components for the nuclei A, and these are reported here for the first time as follows:

$$\sigma_{xx}^{A} = \frac{-K}{\Delta E}\langle r^{-3}\rangle [P_{y_A y_A} + P_{z_A z_A} + \sum_{B}(P_{y_A z_B}P_{y_B z_A} - P_{y_A y_B}P_{z_A z_B})] \quad (4a)$$

$$\sigma_{yy}^{A} = \frac{-K}{\Delta E}\langle r^{-3}\rangle [P_{x_A x_A} + P_{z_A z_A} + \sum_{B}(P_{x_A z_B}P_{x_B z_A} - P_{x_A x_B}P_{z_A z_B})] \quad (4b)$$

$$\sigma_{zz}^{A} = \frac{-K}{\Delta E}\langle r^{-3}\rangle [P_{x_A x_A} + P_{y_A y_A} + \sum_{B}(P_{x_A y_B}P_{x_B y_A} - P_{x_A x_B}P_{y_A y_B})] \quad (4c)$$

$$\sigma_{xy}^{A} = \frac{-K}{\Delta E}\langle r^{-3}\rangle \sum_{B}(P_{z_A z_B}P_{y_A x_B} - P_{z_A x_B}P_{y_A z_B}) \quad (4d)$$

$$\sigma_{xz}^{A} = \frac{-K}{\Delta E}\langle r^{-3}\rangle \sum_{B}(P_{y_A y_B}P_{z_A x_B} - P_{y_A x_B}P_{z_A x_B}) \quad (4e)$$

$$\sigma_{yz}^{A} = \frac{-K}{\Delta E}\langle r^{-3}\rangle \sum_{B}(P_{x_A x_B}P_{z_A y_B} - P_{z_A y_B}P_{z_A x_B}) \quad (4f)$$

where the element of the density matrix are defined by[25]

$$P_{\mu\nu} = \sum_{j}^{occ} C_{\mu j}C_{\nu j} \quad (5)$$

Taking into account that the Me_4Si scale reverses the sign of the shielding scale, the components of the shielding tensors are related to the electronic density matrix by equations of the type

$$\sigma_{\alpha\beta}^{(Me_4Si)} = Af_{\alpha\beta}(P_{\mu\nu}) + B \quad (6)$$

where A is a positive number which depends on K and on the molecular parameters $\langle r^3 \rangle$ and ΔE which for simplicity are taken to be constant for all positions in pyrene. The $f_{\alpha\beta}(P_{\mu\nu})$ are given by eq 4a–f. Equation 6 provides a tool to validate the approximations used in the derivation of eq 4a–f. The success of these approximations is related to the correlation between the calculated electronic density matrix and the measured shielding parameters.

The density matrix was obtained by using the MNDO[26] method and the experimentally determined geometry of pyrene.[13] In Figure 5 the correlation between the calculated and experimental shielding principal values is presented for the in-plane components for all carbon nuclei in pyrene. An excellent correlation is found for the in-plane components ($A = 155.12$, $B = -27.26$ ppm and correlation coefficient $= 0.9914$). This correlation supports the

(21) Schindler, M.; Kutzelnigg, W. *J. Am. Chem. Soc.* **1983**, *105*, 1360.
(22) Ebraheem, K. A. K.; Webb, G. A. *Prog. NMR Spectrosc.* **1977**, *11*, 149.

(23) Pople, J. A. *J. Chem. Phys.* **1962**, *37*, 53.
(24) Pople, J. A. *J. Chem. Phys.* **1962**, *37*, 60.
(25) Pople, J. A.; Beveridge, D. L. *Approximate Molecular Orbital Theory*; McGraw-Hill: New York, 1970.
(26) Dewar, M. J. S.; Thiel, W. *J. Am. Chem. Soc.* **1977**, *99*, 4899.

[13]C Chemical Shielding Tensors

J. Am. Chem. Soc., Vol. 109, No. 9, 1987 2643
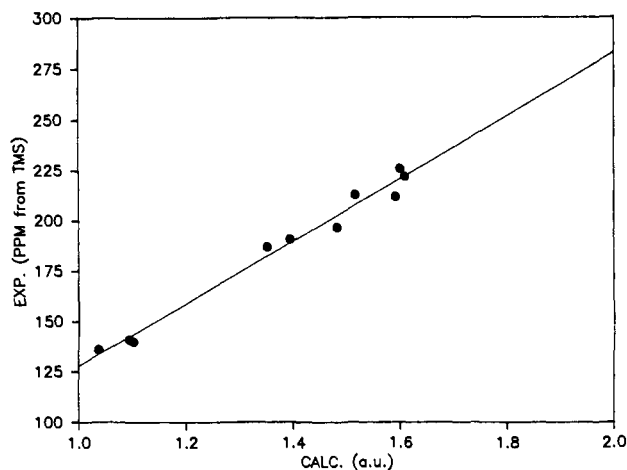
Figure 5. Correlation of calculated and experimental shielding principal values. In-plane components for all pyrene nuclei are shown. An excellent correlation is found (correlation coefficient = 0.9914).

Table I. Experimental and Calculated Values of the ^{13}C Shielding Tensor in Pyrene

	principal^a values				orientation^b of
nuclei	σ_{11}	σ_{22}	σ_{33}	(σ)	principal axes
C_1	212 (220)	141 (142)	21	124.6	$\sigma_{11} = 58°\ (57°)$
C_2	226 (221)	140 (144)	4	123.3	$\sigma_{11} = 0°\ (0°)$
C_4	222 (222)	136 (134)	21	126.3	$\sigma_{11} = 75°\ (77°)$
C_{3a}	213 (208)	187 (182)	−7	131.0	$\sigma_{22} = 12°\ (19°)$
C_{10b}	197 (203)	191 (189)	−18	123.3	$\sigma_{11} = 0°\ (0°)$

^{a} All values in ppm referenced to Me$_4$Si as described in the text. Calculated values are in parentheses. The experimental errors are estimated not to exceed 3 ppm. ^{b} Experimental orientation of component away from the long axis of the molecule. Calculated values are in parentheses.

use of the proposed model to analyze the behavior of the in-plane shielding components in planar fused aromatic rings. No correlation is found for the perpendicular components, σ_{33}, and this is indicative that the MNDO wave functions in the Pople formulation are not adequate to predict these values. The behavior of σ_{33} is determined by factors more complex than those contained in the simple MNDO electronic density matrix.

In Table I the calculated principal values for the in-plane components are compared with the experimental results and found to give excellent agreement between the experimental and calculated values. The agreement between the calculated and experimental orientation of the principal axes of the in-plane shielding components also is quite remarkable considering the approximations used in the formalism. Note that the calculated orientation of the shielding components is independent of the *A* and *B* empirical parameters.

The calculations support the assignment of the resonances of the very similar C_3 and C_4. The ambiguity in the orientation of the in-plane axes for the C_{3a} and C_{10a} is also resolved in that the calculated tensor has the σ_{22} axis at 19° from the long axis oriented as in case I of Figure 4. The experimental orientations of the principal axes verified by calculations are shown in Figure 6.

Discussion

The principal values and axis orientations reported here are averages of the results obtained by fitting the data with no symmetry enforced. For example, the C_1 and C_3 tensors were allowed to vary independently despite the fact that the molecular symmetry requires them to be mirror images of one another. The values are thus subject both to experimental error and to perturbation due to the breaking of the symmetry of the pyrene molecule by intermolecular effects.

In Figure 6, the MNDO[26] calculated bond orders,

$$P_{AB} = \sum_{\substack{\mu \epsilon A \\ \nu \epsilon B}} P_{\mu\nu} \qquad (7)$$
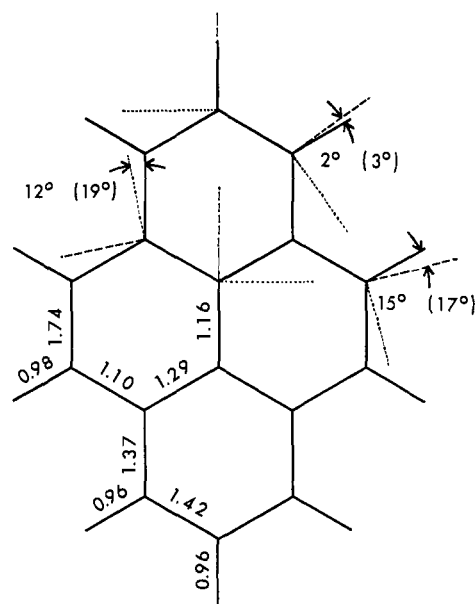
Figure 6. Orientation of the in-plane principal axes and MNDO calculated bond orders. Dashed lines are σ_{11} while dotted lines are σ_{22} and all σ_{33} are perpendicular to the molecular plane. Calculated angles are given in parentheses.

are shown for pyrene. It is apparent from Figure 6 that σ_{11} tends to lie along the bond with the smallest P_{AB} or perpendicular to the bond of largest P_{AB}. All of the values of the P_{CH} are very close to that of benzene ($P_{CH} = 0.96$), and $P_{C_1C_3}$ is close to P_{CC} in benzene ($P_{CC} = 1.41$). It is therefore not surprising that the shielding tensor for C_2 is very similar to the benzene tensor. C_1 also has a shielding tensor very similar to that in benzene, but the calculated σ_{11} principal axis is rotated 2° toward the direction perpendicular to the C_1–C_2 bond. The small deviation can be rationalized by the larger value of $P_{C_1C_2}$ in comparison with $P_{C_1C_{10a}}$ (i.e., the C_1–C_2 has a slightly larger double-bond character than the C_1–C_{10a} bond), supporting the proposal that σ_{11} tends to align along a direction which is perpendicular to the bond of greatest double bond character. In the other protonated carbon, C_4, the differences between the bond orders, $P_{C_{3a}C_4}$ and $P_{C_4C_5}$ is considerably larger, and therefore a deviation of 15° (calculated 17°) from the C–H direction is measured in σ_{11}.

As a general rule it is observed that when two of the three bond orders are equal, σ_{11} will lie along the unique bond if its bond order is the smallest or perpendicular to the unique bond when its bond order is the largest. For the case where all three bond orders exhibit different bond orders, then the σ_{11} axis strikes a compromise between being parallel to the bond with the lowest bond order and perpendicular to the bond with the highest bond order.

The previous rule applies also to the nonprotonated carbons. In the case of C_{10b}, $P_{C_{10b}C_{10c}}$ is smaller than $P_{C_{3a}C_{10b}}$ and $P_{C_{10a}C_{10b}}$, and σ_{11} therefore lies along the C_{10b}–C_{10c} bond as is determined both by calculated and experimental results. In some respects the most interesting shielding reported in this paper is the tensor for C_{3a}. In this case, the results in Figure 6 show that C_{3a}–C_4 has the smallest bond order of bonds attached to C_{3a}. Therefore σ_{11} can be expected to lie closest to the C_{3a}–C_4 direction. Moreover, as $P_{C_3C_{3a}}$ is larger than $P_{C_{10b}C_{3a}}$, there is a small deviation of 19° (calculated 12°), of σ_{11} from the C_{3a}–C_4 direction toward the direction perpendicular to the C_3–C_{3a} bond.

Conclusions

The quantitative analysis of the in-plane shielding components in terms of the MNDO bond orders establishes a clear relationship between the orientation of the ^{13}C shielding and the character of the C–C bonds, providing a tool for the analysis of ^{13}C shielding tensor in molecules with fused aromatic rings. The excellent agreement between the calculated and experimental values for the in-plane shielding components supports the assignment presented here and the use of the Pople model to rationalize the

in-plane shielding components. Unfortunately, the present model cannot be applied to the perpendicular component σ_{33}, which is determined by factors more complex than the bond orders. It is apparent that the values of σ_{33} are consistent with the qualitative predictions of the ring current model[27], but a detailed analysis is deferred until a more extensive theory can be applied to a molecule of this size.

The results presented here for a fused aromatic molecule point toward an important method to assess the relative aromaticity of the individual bonds in a molecule. Contrary to other techniques,[9] which focus on the molecule as a whole, the measurement of ^{13}C shielding tensors in polycyclic aromatic compounds presents a premier tool for the analysis of the aromatic character of individual bonds in the molecule. The rules established here correlate

the degree of aromaticity of the adjacent bonds with the ^{13}C measured shielding tensors in pyrene. Moreover, this rule holds for a large number of polycyclic aromatic compounds studied theoretically.[28]

The richness of the full tensor description of chemical shielding in pyrene stands in sharp contrast to the liquid results where all of the observed lines are within 7 ppm of one another, illustrating once more the power of modern NMR of solids.

(27) Haigh, C. H.; Mallion, R. B. *Prog. NMR Spectrosc.* **1980**, *13*, 303.

(28) Facelli, J. C.; Grant, D. M. *Theor. Chim. Acta*, in press.

Spin Coupling in Metalloporphyrin π-Cation Radicals

Brian S. Erler, William F. Scholz, Young Ja Lee,[1] W. Robert Scheidt,*[1] and Christopher A. Reed*

Contribution from the Departments of Chemistry, University of Southern California, Los Angeles, California 90089-1062, and University of Notre Dame, Notre Dame, Indiana 46556. Received August 8, 1986

Abstract: The magnetic interactions between metal and ligand spins in metalloporphyrin π-cation radicals have been investigated as a function of d orbital type for synthetically accessible $S = 1/2$ metals from the first transition series. Most instructive is the case of copper(II) where the presumably planar $[Cu(TMP^\bullet)]^+$ ($TMP^\bullet = \pi$-cation radical of tetramesitylporphyrinate) has an overall $S = 1$ state ($\mu_{eff} = 2.99 \mu_B$). The ferromagnetic coupling of spins is rationalized as arising from the exchange interaction of unpaired electrons in orthogonal magnetic orbitals. By contrast, $[Cu(TPP^\bullet)]^+$ has a ruffled porphyrin core in the solid state and is diamagnetic ($S = 0$). The antiferromagnetic coupling is rationalized in terms of overlap of the magnetic orbitals, i.e., bond formation with spin pairing in the bonding molecular orbital. The same principles seem to apply to the analogous systems of V(IV), Co(II), and low-spin Fe(III), where in each case the metal unpaired electron is in a different d orbital. Some reinterpretation of previous conclusions is required. The crystal and molecular structure of $[Cu(TPP^\bullet)][SbCl_6]$ has been determined. The structure consists of $[Cu(TPP^\bullet)]^+$ ions that interact in pairs in the crystalline lattice. Dimer formation is believed to be the cause of the exceptionally small dihedral angles between the peripheral phenyl rings and the porphinato core (average value 41.5°). This dimerization is also responsible for the unusual saddle-shaped core conformation. This conformation has also been observed in other π-cation radical species. The observed Cu–N bond distance of 1.988 (4) Å is typical of that for copper(II) and confirms the ring-oxidized nature of the compound. Crystal data: $a = 13.484$ (2) Å, $b = 13.924$ (3) Å, $c = 12.886$ (2) Å, $\alpha = 98.90$ (2)°, $\beta = 111.08$ (1)°, $\gamma = 106.97$ (2)°, triclinic, $P\bar{1}$, $Z = 2$, $CuN_4C_{44}H_{28}SbCl_6$. The ultimate simplicity and apparent generality of the spin-coupling theory provide one of the most accessible and heuristically useful entries to understanding the fundamental concepts of magnetic coupling phenomena.

In a recent paper on iron(III) porphyrin π-cation radical complexes[2] we proposed a theory to account for the notable difference in coupling of metal and ligand spins in Fe(OClO$_3$)$_2$(TPP$^\bullet$) and $[FeCl(TPP^\bullet)]^+$ (TPP$^\bullet$ = π–cation radical of tetraphenylporphyrinate).[3] Spin coupling in the former is ferromagnetic. In the latter it is antiferromagnetic. The theory is based on the occupations and symmetries of the so-called magnetic orbitals, i.e., those orbitals on the metal and the ligand that contain an unpaired electron. The diversity of d orbital occupations and symmetries across the first transition series provides an excellent opportunity to probe the scope and generality of this theory. Metalloporphyrin π-cation radical complexes whose half-occupied d orbitals are strictly orthogonal to the porphyrin π-radical orbital are expected to show ferromagnetic coupling (like Hund's rule). Thus, the spin state of higher multiplicity will be

lower in energy. For example, in a strictly planar environment of D_{4h} symmetry, $Cu^{II}(porph^\bullet)$ would have orthogonal metal ($d_{x^2-y^2}$) and ligand (a_{1u} or a_{2u}) magnetic orbitals and be expected to show an $S = 1$ (i.e., triplet) ground state. On the other hand, complexes whose metal and ligand magnetic orbitals are not strictly forbidden by symmetry to overlap are expected to show *antiferro*magnetic coupling (or bond formation). The spin state of lower multiplicity will be lower in energy. For example, in a nonplanar environment of say C_{2v} symmetry, $Cu^{II}(porph^\bullet)$ would be expected to have an $S = 0$ (i.e., singlet) ground state. Earlier[4] we noted the existence of the latter state in the diamagnetic crystalline solid $[Cu(TPP^\bullet)][SbCl_6]$, and we now present evidence for the antithetic case in the mesityl analogue $[Cu(TMP^\bullet)][SbCl_6]$. We also explore the syntheses and properties of π-cation radical complexes of V, Co, and Ni. Like copper, the vanadyl and cobalt cases provide $S = 1/2$ metals, but the particular half-occupied d orbital is different in each case. These studies lead to a reinterpretation of certain published data and suggest there may be

(1) University of Notre Dame.
(2) Gans, P.; Buisson, G.; Duée, E.; Marchon, J.-C.; Erler, B. S.; Scholz, W. F.; Reed, C. A. *J. Am. Chem. Soc.* **1986**, *108*, 1223.
(3) Abbreviations used in this paper: TPP = tetraphenylporphyrinate, OEP = octaethylporphyrinate, TMP = tetramesitylporphyrinate, and SCE = saturated calomel electrode.

(4) Scholz, W. R.; Reed, C. A.; Lee, Y. J.; Scheidt, W. R.; Lang, G. *J. Am. Chem. Soc.* **1982**, *104*, 6791–6793.